Chinese Journal of Chemical Engineering 28 (2020) 1744–1751

Contents lists available at ScienceDirect

Chinese Journal of Chemical Engineering

journal homepage: www.elsevier.com/locate/CJChE

Article

High-gravity-assisted green synthesis of rare-earth doped calcium molybdate colloidal nanophosphors

Yuan Pu [1,2], Lifeng Lin [1,2], Jun Liu [1,2], Jiexin Wang [1,2], Dan Wang [1,2,*]

[1] State Key Laboratory of Organic Inorganic Composites, Beijing University of Chemical Technology, Beijing 100029, China
[2] Research Center of the Ministry of Education for High Gravity Engineering and Technology, Beijing University of Chemical Technology, Beijing 100029, China

ARTICLE INFO

Article history:
Received 18 February 2020
Received in revised form 9 March 2020
Accepted 12 March 2020
Available online 21 March 2020

Keywords:
Colloidal nanophosphors
$CaMoO_4$
Process intensification
High gravity technology
Green solvent

ABSTRACT

In this work, we report an innovative route for the synthesis of rare-earth doped calcium molybdate ($CaMoO_4$) nanophosphors by using high gravity rotating packed bed (RPB) technology and paraffin liquid as the solvent. The significant intensified mass transfer and micromixing of reactants in the RPB reactor are benefiting for homogeneous doping of rare-earth ions in the host materials, leading to nanophosphors with high quantum efficiency. The use of liquid paraffin as the solvent eliminates the safety risks associated with volatile organic compounds, increasing the potential for clean production of nanophosphors. Under excitation of deep ultraviolet (DUV) light, the $CaMoO_4$:Na^+, Eu^{3+} nanophosphors exhibit red emission at peak wavelength of 615 nm and quantum yield of up to 35.01%. The $CaMoO_4$:Na^+,Tb^{3+} nanophosphors exhibit green emission at peak wavelength of 543 nm with quantum yield of up to 30.66%. The morphologies of the nanophosphors are tunable from nanofibers through nanorods to nanodots and the possible mechanism of controlling the formation of different nanostructures is proposed on the basis of experimental results and theoretical analysis of mesoscience. These nanophosphors are highly dispersible in organic solvents and utilized for fabricating fabrication of flexible, free-standing luminescent films based on silicone resin. We also demonstrate the red LEDs consisting of the hybrid films of $CaMoO_4$:Na^+,Eu^{3+} nanoparticles as color-converting phosphors and DUV LEDs as illuminators, offering strong potential for future nanophosphors-basedsolid-state lighting systems.

1. Introduction

The rare-earth doped functional inorganic nanoparticles, which generally consist of inorganic crystalline hosts and rare-earth ions doped in the lattice of the nanocrystals, have found many applications in biomedical and energy related areas [1–4]. The unique light converting properties of doped rare-earth ions enable the nanoparticles to be nanophosphors for optical bioimaging [5] and optoelectronic devices [6,7]. Since the deep ultraviolet (DUV) light-emitting diodes (LEDs) are in demand for a wide variety of area including sterilization, water purification and biomedical applications in recent years, the development of nanophosphors that can be efficiently excited in the DUV range has been a hot topic [8,9]. After trial treatment and using the appropriate methods, the nanophosphors can be processed into transparent plastics composites with high polymer material, utilized for lighting and flexible display devices based on DUV LEDs [10,11].

The rare-earth activated calcium molybdate ($CaMoO_4$) nanophosphors are among the most promising candidates for green and red emitting phosphors, due to their good chemical stability and excellent fluorescence characteristics under DUV light excitation [12–16]. To date, various synthesis routes have been adopted to control the shape and improve the properties of rare earth doped $CaMoO_4$ phosphors, including auto-combustion [17], microwave synthesis [18], and hydrothermal treatment followed by annealing [19–21]. Nevertheless, most of the synthetic routes require high temperature (>700 °C) treatment, resulting in the aggregates of particles. The fabrication of free-standing luminescent films based on $CaMoO_4$ colloidal nanophosphors is challenging. Recently, Ding *etal.* [22] developed the synthesis approach to RE^{3+}(RE = Eu, Sm, Dy, Tb)-doped $CaMoO_4$ *via* the supersaturated recrystallization method by using dimethylformamide (DMF) as the solvent, while using oleylamine and oleic acid as the surface ligands. The obtained nanophosphors exhibited fiber morphologies with the length ranging from 40 to 70 nm and width of 2 nm, showing strong luminescence without any post-thermal treatments [22]. The supersaturated recrystallization method offers the potential for large-scale production of $CaMoO_4$ based colloidal nanophosphors. Although DMF has been one of the common solvents used in the industry, it is easily absorbed through the skin and by inhalation and ingestion. The

* Corresponding author at: State Key Laboratory of Organic Inorganic Composites, Beijing University of Chemical Technology, Beijing 100029, China.
E-mail address: wangdan@mail.buct.edu.cn (D. Wang).

https://doi.org/10.1016/j.cjche.2020.03.023
1004-9541/

wastewater containing DMF shows low biodegradability, high toxicity and stability, which is harm to human health and environment. As the green chemistry concept is growing rapidly, the issues related to the solvent selection need consideration at the early stage of the study [23,24]. Green synthesis of nanophosphors requires reducing the use of products from raw materials to final disposal of the entire life cycle of the adverse effects. Along with others, we have developed the synthesis of semiconductor quantum dots and lanthanide-dopedrare-earth fluorides by using ecofriendly liquid paraffin as the solvent [25–27]. Compared with commonly used organic solvents such as DMF, toluene and octadecene, the liquid paraffin is greener and more sustainable choice as the solvent for chemical synthesis. However, the synthesis of nanophosphors is a complex combination of a series of unit operations such as mixing of the reactants, formation of particles and separation of products. To obtain nanophophors with controllable morphologies and uniform size distributions, particular attention should be paid to the mixing of the reactants and precipitation rate difference of various ions [28,29].

In this work, we develop an innovative route for the synthesis of $CaMoO_4$:Na^+,Eu^{3+} and $CaMoO_4$: Na^+,Tb^{3+} nanophosphors *via* by using high gravity rotating packed bed (RPB) technology and paraffin liquid as the solvent. The morphology, structure and optical properties of the nanophosphors are investigated by transmission electron microscope (TEM), powder X-ray diffraction (XRD), Fourier transform infrared (FTIR) spectrophotometry, thermogravimetric analysis (TGA), luminescence spectra and luminescent quantum yield measurements. The possible mechanism of the formation of different nanostructures is proposed. The preliminary applications of the nanophosphors for freestanding luminescent films and LED devices are demonstrated.

2. Experimental

2.1. Materials

Calcium nitrate ($Ca(NO_3)_2$), erbium trinitrate pentahydrate ($Eu(NO_3)_3\cdot 6H_2O$), dysprosium nitrate ($Tb(NO_3)_3$), sodium nitrate ($NaNO_3$), sodium oleate ($C_{17}H_{33}CO_2Na$) and ammonium molybdate tetrahydrate ($(NH_4)_6Mo_7O_{24}\cdot 4H_2O$) were purchased from Macklin Biochemical Co., Ltd. (Shanghai, China), whose purities were 99.9% metal basis. The oleic acid, oleylamine, liquid paraffin, toluene and ethanol were purchased from Sinopharm Chemical Reagent Co., Ltd. (Beijing, China). All the chemicals are used without any additional purification unless otherwise mentioned. Deionized water is used for all experiments. The commercial silicone resin supplied as a two-part A/B kit (OE-6336, Dow Corning) was used for the preparation of freestanding luminescent film. The commercial DUV LED chips (B44LD7A1CS0, Tianjin Henglong Technology Co, Ltd) with emission in the range of 265–275 nm was used for the illuminators of LED devices.

2.2. Synthesis of $CaMoO_4$:Na^+,Eu^{3+}(Tb^{3+}) nanophophors

An internal circulation RPB reactor [30,31] consisting of a packed rotator, a motor, a temperature-control jacket, a seal ring, a lifter, an inlet and an outlet, was used for the mixing of the reactants and supersaturated recrystallization of the rare earth doped $CaMoO_4$ nanoparticles. Typically, 3.84 mol calcium nitrate, 0.08 mol erbium trinitrate pentahydrate (dysprosium nitrate), 0.08 sodium nitrate and 2.679 g sodium oleate were dissolved in 40 ml water in a 500 ml beaker, followed by the addition of 60 ml liquid paraffin , 10 ml oleic acid and 10 ml oleylamine with vigorous stirring to form solution A. 0.57 mol of ammonium molybdate tetrahydrate was dissolved in 20 ml water in a 100 ml flask to form solution B. The two solutions were simultaneously added into the RPB reactor and the mixture was then allowed for reaction at 80 °C in the internal circulation RPB reactor operating on a certain high gravity level (rotation speed of packing in the RPB reactor) for 5 h. Then, the reaction mixture was cooled and the water was removed by vacuum distillation. The oil phase was then added with excess ethanol and the precipitates were collected by centrifugation. After washing with ethanol for three times, the obtained nanophosphors of $CaMoO_4$:Na^+,Eu^{3+}(Tb^{3+}) were dried in a vacuum oven. The effects of the rotation speeds of packing in the RPB reactor (1000 r·min^{-1}, 1500 r·min^{-1}, 2000 r·min^{-1} and 2500 r·min^{-1}, respectively), the volume ratio of liquid paraffin/water (2:1, 1:1, 1:2) and oleic acid/oleylamine (3:1, 1:1, 1:3), were investigated.

2.3. Fabrication of freestanding luminescent films

A certain amount of the purified nanophosphors of $CaMoO_4$:Na^+, Eu^{3+}, A kit and B kit resin were diluted with toluene and vortexed until the well combined. The hybrid dispersion was poured into the Teflon mold and maintained in vacuum drier for 10 h to remove air bubbles and the toluene. The freestanding luminescent film was then obtained by curing the silicone resin at 130 °C for 2 h. The resulting 1 mm thick freestanding luminescent film (2 cm × 2 cm) was then peeled off from the Teflon mold for further characterization. The hybrid films with $CaMoO_4$:Na^+,Eu^{3+} contents of 0, 0.2wt%, 0.4wt%, 0.8wt%, 1.6wt%, and 3.2 wt% were prepared, respectively.

2.4. Characterization

The morphologies of the nanophosphors were investigated by a Hitachi H-7700TEM working in bright-field mode. The XRD patterns of the samples were measured by a Bruker D8 Discover XRD diffractometer. A Nicolet 6700 FTIR spectroscopy was used to record the FITR spectra of the nanophosphors. Optical properties of samples were collected on a Laser Flash-photolysis Spectrometer (Edinburgh Instruments).

3. Results and Discussion

The formation process of $CaMoO_4$ nanoparticles is shown schematically in Fig.1. The reactive precipitation and supersaturated recrystallization of $CaMoO_4$ occurred in a high gravity RPB reactor. The liquid paraffin is used as the solvent, enabling the control of reactivity for liquid-phase reactions. The oleic acid and oleylamine act as the surfactants for controlling the crystallization growth of the nanocrystals. Due to the high gravity environment and porous structure of the packing inside the RPB, the liquid is distorted, breaks up, and becomes separated tiny droplets. The mass transfer and micromixing of the reactants were significantly intensified and the two phases of water and paraffin were rapidly emulsified to form small droplets, which then acted as micro-reactors for the formation of nanoparticles. The Ca^{2+} ions passivated by the coordination of oleic acid and oleylamine in the oil phase arranged to the aqueous phase side and immediately reacted with MoO_4^{2-} in the aqueous phase at the interface. The $CaMoO_4$ crystal nuclei were then generated and further grew to form ligand-coated $CaMoO_4$ nanocrystals at 80 °C for 5 h. The RE^{3+} (RE = Eu, Tb) ions and Na^+ ions were simultaneously doped into the nanocrystals. The unique advantage of RPB in intensifying the mass transfer and micromixing of reactants maximized the possibility of homogenous surfactant distribution and supersaturation in whole processing, leading to homogeneous doping of rare-earth ions in the host materials and enabling the formation of high quantum efficiency nanophosphors.

The effects of rotation speeds of packings in the RPB reactors on the morphologies of the $CaMoO_4$ nanoparticles were firstly evaluated. The atom ratio of Ca^{2+}:Na^+:Eu^{3+} was 0.58:0.21:0.21. The reaction time in the RPB reactors was 5 h and the reaction temperature was 80 °C. The volume ratio of liquid paraffin/water was 1:1 and the volume ratio of oleic acid/oleylamine was 1:1. The rotation speeds of packings in the RPB reactors were set as 1000 r·min^{-1}, 1500 r·min^{-1}, 2000 r·min^{-1} and 2500 r·min^{-1} respectively. Fig.2a–d shows the corresponding TEM images of the samples prepared in RPB reactors operating with rotation speeds of 1000 r·min^{-1}, 1500 r·min^{-1}, 2000 r·min^{-1} and

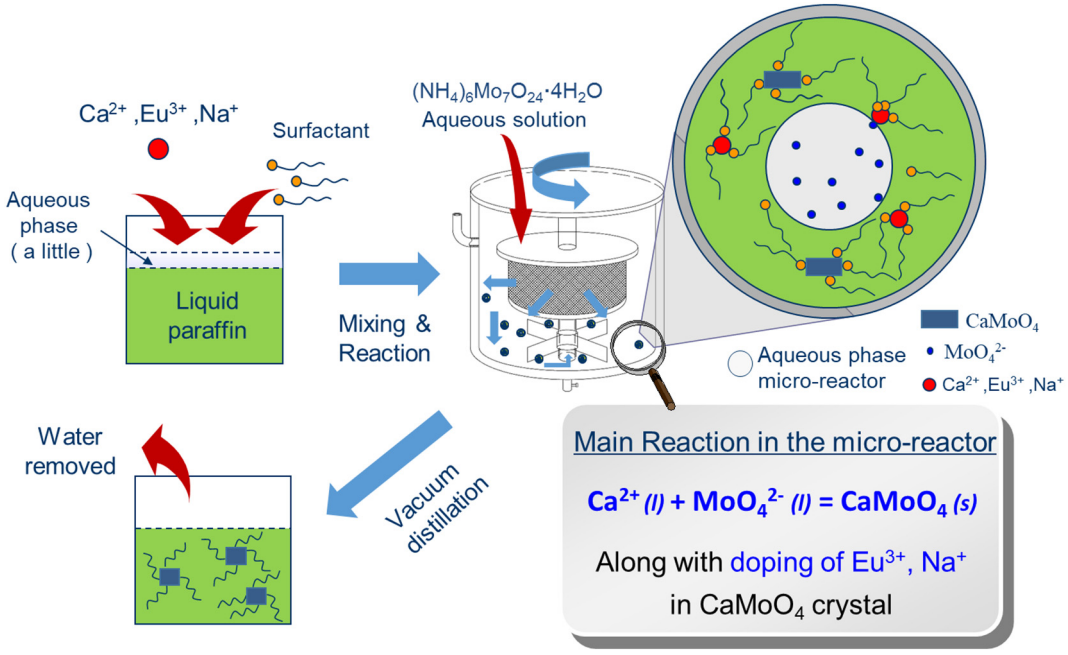

Fig.1. Schematic diagram for the main process $CaMoO_4$ nanoparticles formation.

2500 r·min^{-1}, respectively. When the rotation speed was 1000 r·min^{-1}, the morphology of the obtained $CaMoO_4$ nanoparticles was nanofibers with the length larger than 100 nm and width of around 3 nm. According to the TEM images, the obtained nanofibers were more like nanochains from nanocrystal self-assembly*via*shape-directed nanoparticle attachment, straightening, and orientation correction [32]. As the rotation speed increased to 1500 r·min^{-1}, the obtained $CaMoO_4$ nanoparticles still exhibited fiber morphology, while of the fibers was much shorter, with average length of 50 nm. As the rotation speeds further increased to 2000 r·min^{-1} and 2500 r·min^{-1}, the obtained $CaMoO_4$ nanoparticles showed similar nanorod morphologies. These results revealed that the morphologies of the nanophosphors are tunable from nanofibers to nanorods by controlling the rotation speeds of the RPB reactor.

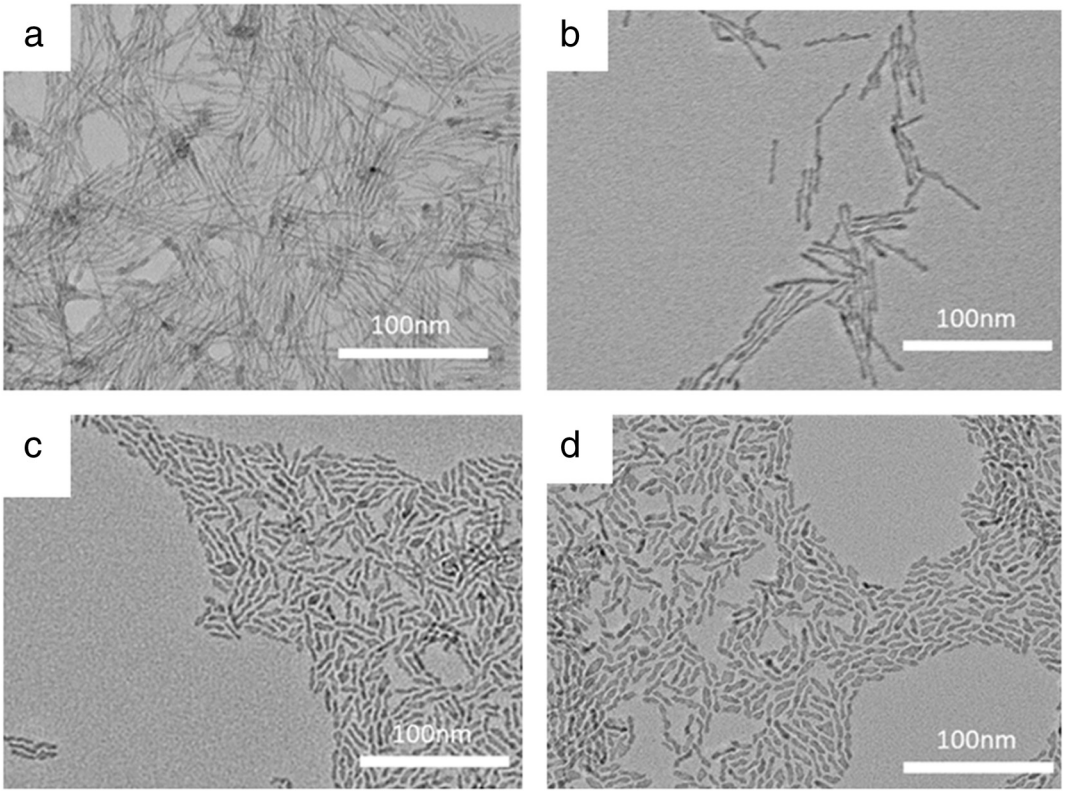

Fig.2. TEM images of rare-earth doped $CaMoO_4$ nanoparticles obtained in RPB reactors operating with rotation speeds of (a)1000 r·min^{-1}, (b)1500 r·min^{-1}, (c)2000 r·min^{-1} and (d) 2500 r·min^{-1}.

The schematic diagram of the process and possible chemical reactions involved in the formation of the $CaMoO_4$ nanoparticles in the oil–water interface were shown in Fig. 3. Due to the limitation of mass transferring at the nanoscale, it is hard to realize the coating of surfactants simultaneously on all faces of single nanoparticle. At the oil–water interface, the structure change of the $CaMoO_4$ nanoparticle is jointly controlled by two dominant mechanisms of homogeneous nucleation (mechanism A)and nanocrystal self-assembly (mechanism B), which can be considered as a typical mesoregime [33]. In the regime of our work, the competition between mechanism A and mechanism B mainly relies on the interphase renovation rate of the oil–water interface and the anions (MoO_4^{2-}) diffusion rate across the oil–water interface. According to the concept and logic of mesoscience, the transition between the A,A-B, and B regimes was accompanied by sudden changes in the system's characteristics and function [34,35]. In the case that the interphase renovation rate of the oil–water interface is less than the anions (MoO_4^{2-}) diffusion rate, mechanism A weakens and mechanism B dominates the system, resulting in long nanofibers of from nanocrystal self-assembly including shape-directed nanoparticle attachment, straightening, and orientation correction. In opposite situation that the interphase renovation rate is significantly enhanced and faster than that of the anions (MoO_4^{2-}) diffusion rate, mechanism A dominates the system and mechanism B weakens, resulting in short $CaMoO_4$ nanorods. Therefore, by increase the rotation speed of the RPB reactor to enhance the interphase renovation rate of the oil–water interface in the system, the obtained $CaMoO_4$ varied from nanofibers to nanorods.

In addition to the rotation speeds of the reactor, the volume ratio of liquid paraffin/water and oleic acid/oleylamine in the synthesis processing also exhibited significant effects on the structure of nanophosphors products. Fig. 4a and b shows the typical TEM images of the $CaMoO_4$ nanoparticles when the volume ratios of oleic acid/oleylamine were 3:1 and 1:3 respectively. According to previous study, the oleylamine molecules could promote the deprotonation of oleic acid into $C_{17}H_{33}COO^-$, which enable the strong and dense selective adsorption of the deprotonated oleic acid onto certain facets of inorganic nanocrystals [36]. Therefore, along with the decreasing of oleic acid/oleylamine ratio, the coating of surfactants on the nanoparticles was more easy and the reactants in the system were more likely to form short nanorods (Fig. 4b), rather than nanofibers (Fig. 4a). Fig. 4c and d presents typical TEM images of the $CaMoO_4$ nanoparticles when the volume ratios of liquid paraffin/water were 2:1 and 1:2 respectively. As the ratio of liquid paraffin/water decreases, the interface concentration of anions in the water phase and the diffusion rate of anions across the oil–water interface reduced correspondingly. According to the above-mentioned analysis based on the mesoscience, the mechanism A that was homogeneous nucleation was strengthened and dominated the system, resulting to ultrasmall nanodots of $CaMoO_4$ (Fig.4d). Fig.4e shows the typical XRD curve of the obtained nanoparticles, indicating the crystalline structure of scheelite type $CaMoO_4$, which is in good agreement with standard JCPDS file number 85-1267. The FTIR spectrum in Fig.4f demonstrated the presence of organic surfactants, in which the characteristic peaks of COO— symmetric stretch from oleic acid were observed at 1550 and 1442 cm^{-1}. Therefore, the newly developed synthesis route for the synthesis of $CaMoO_4$ by using high gravity technology for process intensification and paraffin liquid as the solvent enables the controlling of product morphologies from nanofibers through nanorods to nanodots. In addition, unlike the previous reported synthesis methods, the use of liquid paraffin as the solvent eliminates the safety risks associated with volatile organic compounds and offers a green synthetic route, which may increase the potential for large-scale production of rare-earth doped nanophosphors.

The photoluminescence (PL) is one of the fascinating features of nanophosphors, which make them attractive for various applications. For rare earth doped nanophosphors, the luminescent properties are extremely sensitive to their mesoscale structures, such as concentration and distribution of defects and doping ions [37]. The PL spectra of $Ca_{(1-2x)}MoO_4{:}xNa^+,xEu^{3+}$ (x = 0.01, 0.02, 0.03, 0.05, 0.10) and $Ca_{(1-2x)}MoO_4{:}xNa^+,xTb^{3+}$ (x = 0.01, 0.02, 0.03, 0.05, 0.10) nanophosphors under the same 263 nm DUV light excitation were shown in Fig.5. It is obvious that the Eu^{3+} doped $CaMoO_4$ nanophosphors exhibited red emission with peak wavelength of 615 nm and the optimized doping concentrations of Eu^{3+} was 2 atom%. Tb^{3+} doped $CaMoO_4$ nanophosphors exhibited green emission with peak wavelength of 615 nm and the optimized doping concentrations of Tb^{3+} was 3 atom%.

Fig.6 shows that both powders and dispersions of the nanophosphors exhibited bright luminescence under the excitation of DUV light *via*254 nm DUV lamps. Fig.6b and e also demonstrated that

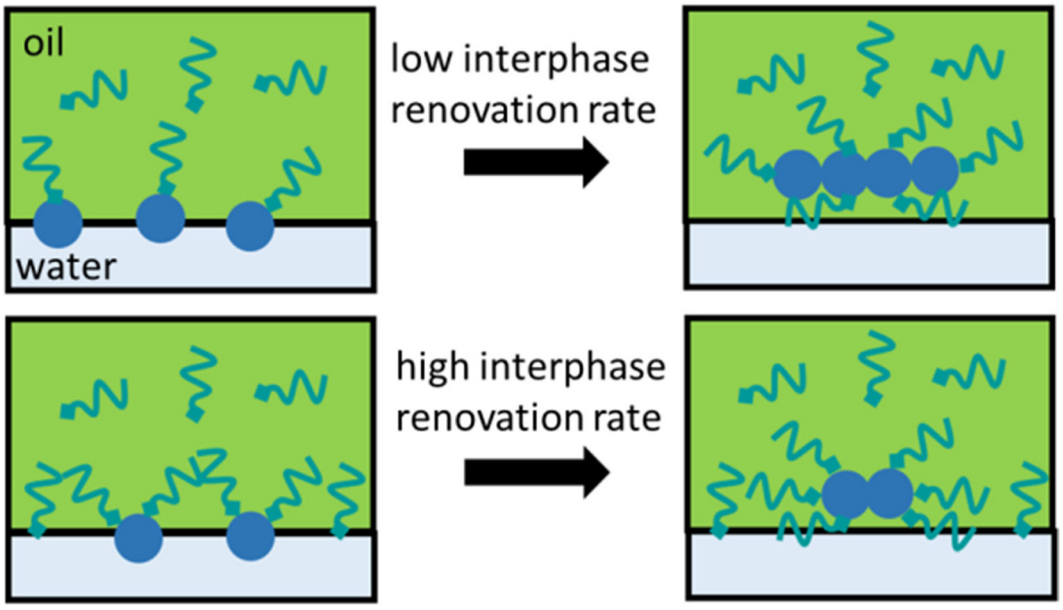

Fig.3. Schematic diagram of the process and possible chemical reactions involved in the formation of the $CaMoO_4$ nanoparticles in the oil–water interface with low and high interphase renovation rates, respectively.

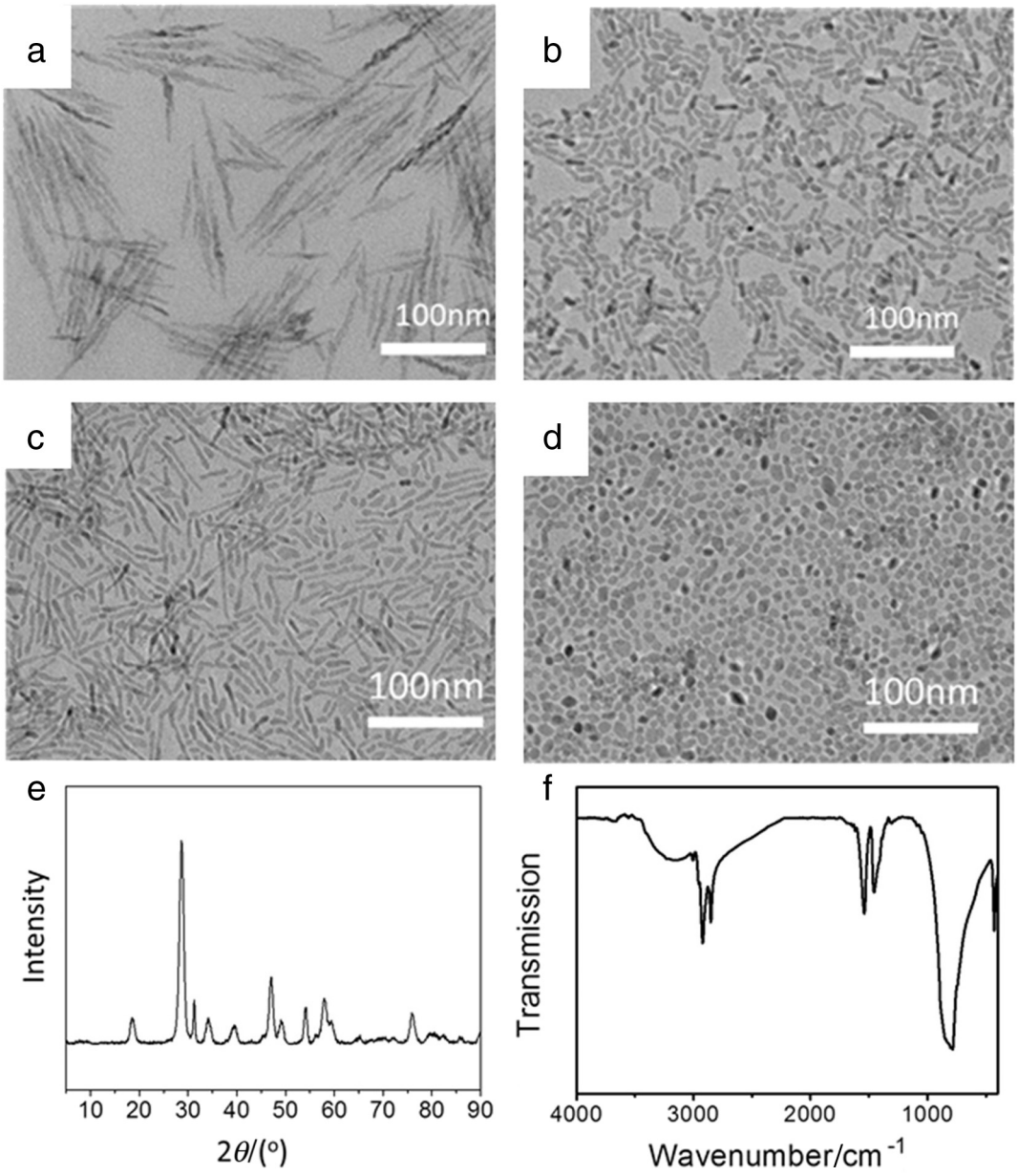

Fig.4. TEM images of rare-earth doped $CaMoO_4$ nanoparticles obtained under different experimental conditions. Volume ratios of oleic acid/oleylamine were (a)3:1 and (b)1:3 while the volume ratio of liquid paraffin/water was 1:1. Volume ratios of liquid paraffin/water were (c)2:1 and (d)1:2 while the volume ratio of oleic acid/oleylamine was 1:1. The rotation speeds are 2000 $r \cdot min^{-1}$ for the four experiments. (e)XRD curve and (f)FTIR spectrum of the rare-earth doped $CaMoO_4$ nanoparticles.

the nanophosphors could disperse well in organic solvents, enabling them for light-converting "transparent" fillers in polymer based freestanding luminescent films. Fig.6c and f presents the CIE coordinates of $Ca_{0.96}MoO_4$:0.02Na^+,0.02Eu^{3+} nanophosphors and $Ca_{0.94}MoO_4$:0.03Na^+,0.03Tb^{3+} phosphors. The CIE coordinates of Eu^{3+} doped $CaMoO_4$ nanophosphors were (0.60469 0.35001), which were in the red region. The Tb^{3+} doped $CaMoO_4$ nanophosphors exhibited typical green emission with CIE coordinates of (0.28538 0.58959). The luminescent quantum yield of $CaMoO_4$:Na^+,Eu^{3+} nanophosphors and $CaMoO_4$:Na^+,Tb^{3+} nanophosphors was 35.01% and 30.66%, respectively. As a comparison, Ding *et al.* [22] reported the quantum yields of 25.7% for $CaMoO_4$:Na^+,Eu^{3+} nanofibers and 27.7% for $CaMoO_4$:Na^+, Tb^{3+} nanofibers. The nanophosphors obtained in our work were smaller than the nanofibers and exhibited higher quantum yields, which were attributed to the significant intensified mass transfer and micromixing of reactants in the RPB reactor, leading to homogeneous doping of rare-earth ions in the host materials and resulting in nanophosphors with high luminescent quantum efficiency.

In order to explore the potential functions and applications of rare earth doped $CaMoO_4$ nanophosphors, we fabricated hybrid films of silicone/$CaMoO_4$:Na^+,Eu^{3+} *via* co-solvent methods. As shown in Fig.7a and b, the hybrid films were nearly transparent under daylight and exhibited bright red luminescence under DUV light excitation, even though the weight ratios of the nanophosphor were at low levels. As the weight ratios of $CaMoO_4$:Na^+,Eu^{3+} in the hybrid films from 0.2% to 3.2% increases, the luminescence intensity increased without aggregation caused quenching. In addition, Fig.7c shows a typical LED lamp fabricated by using a commercial DUV LED chip with emission in the range of 265–275 nm and the silicone/$CaMoO_4$:Na^+,Eu^{3+} hybrid film as the encapsulation layer. After the device was powered on, obvious red light was observed, and the luminescence spectrum shown in Fig.7d agreed well with that of $CaMoO_4$:Na^+,Eu^{3+} powder.

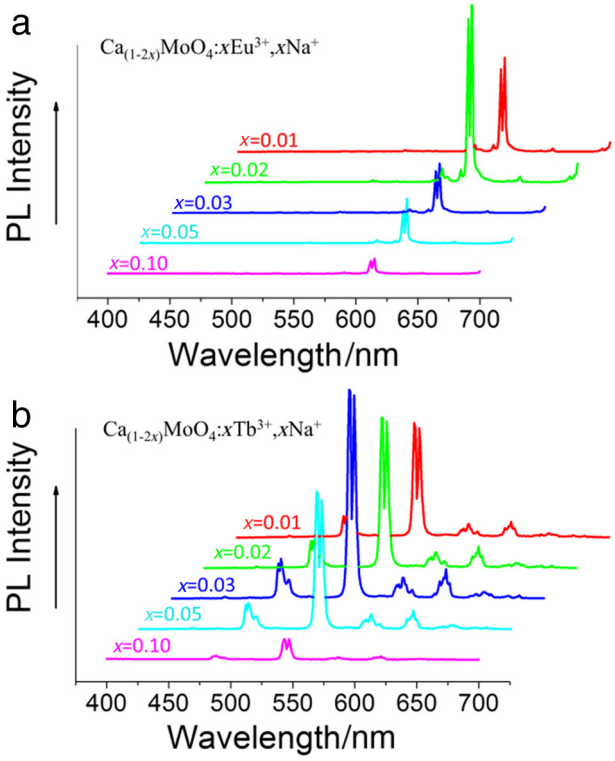

Fig.5. DUV excited PL intensity of (a)$Ca_{(1-2x)}MoO_4$:xNa^+,xEu^{3+} and (b)$Ca_{(1-2x)}MoO_4$:xNa^+,xTb^{3+} nanophosphors with different doping concentrations of rare earth ions. x = 0.01, 0.02, 0.03, 0.05, 0.10 respectively. $\lambda_{Excitation}$ = 263 nm.

4. Conclusions

Along with the rapid development of LED lighting and display, green and scalable synthesis approaches of high performance nanophosphors are highly required. In this work, we demonstrate an innovative route for the synthesis of rare-earth doped $CaMoO_4$ nanophosphors by using high gravity technology for process intensification and paraffin liquid as the green solvent. The morphologies of the nanophosphors are tunable from nanofibers through nanorods to nanodots by controlling the experimental conditions. The mechanism of controlling the formation of different nanostructures in the RPB reactor was proposed, as inspired by the concept of "mesoscience". The luminescent quantum yield of obtained red nanophosphors reached to 35.01% with CIE coordinates of (0.60469 0.35001) and peak emission wavelength at 615 nm. The green nanophosphors exhibited luminescent quantum yield of up to 30.66% with CIE coordinates of (0.28538 0.58959) and peak emission wavelength at 543 nm. Compared to traditional synthesis approaches using the stirred reactors (STRs), the significant intensified mass transfer and micromixing of reactants in the RPB reactor are benefiting for homogeneous doping of rare-earth ions in the $CaMoO_4$ host materials, leading to nanophosphors with high quantum efficiency. The use of liquid paraffin as the solvent eliminates the safety risks associated with volatile organic compounds and offers a green synthetic route, which may increase the potential for large-scale production of rare-earth doped nanophosphors. The nanophosphors were highly dispersible in organic solvents and were used for fabricating fabrication of flexible, freestanding luminescent films based on silicone resin. The red LED lamp consisting of DUV LED chip as the illuminator and the hybrid films of silicone/$CaMoO_4$:Na^+,Eu^{3+} as encapsulation layer were prepared.

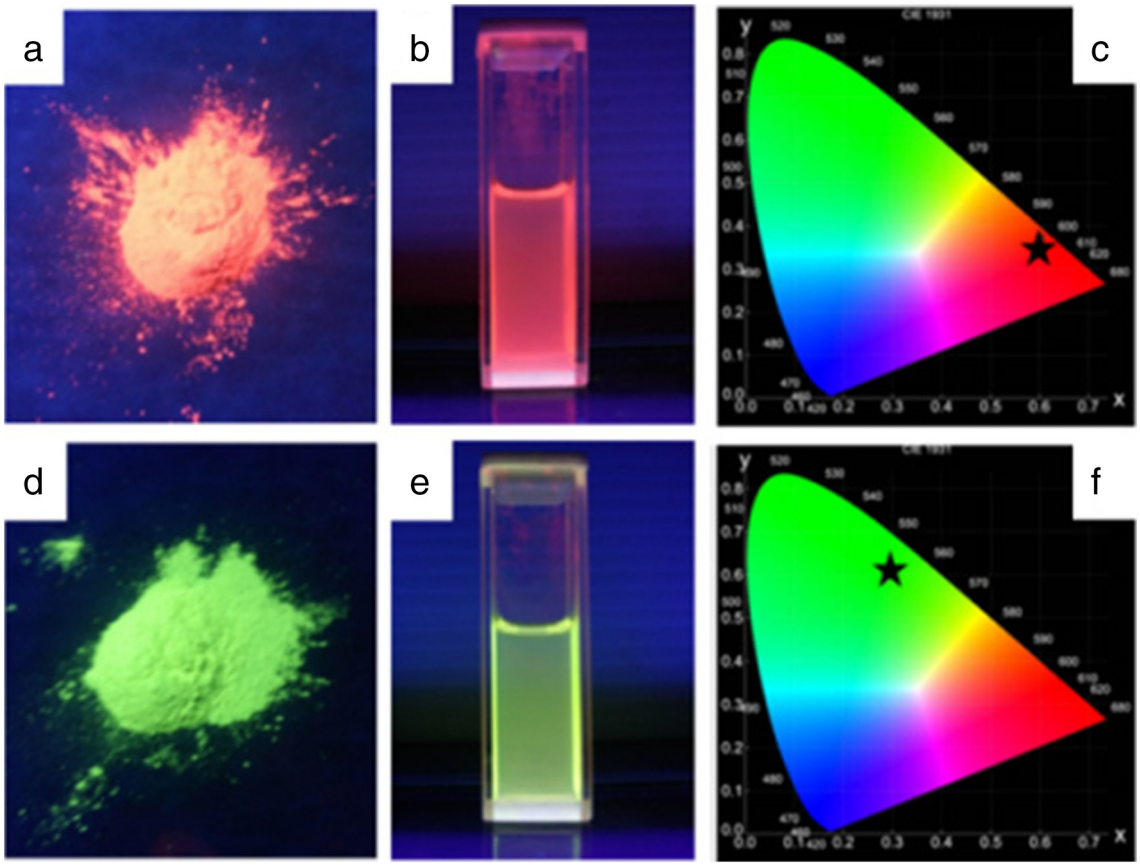

Fig.6. Photographs of (a, d)powders, dispersions in toluene (5 mg·ml^{-1}) and CIE chromaticity maps of (a–c) $Ca_{0.96}MoO_4$:$0.02Na^+$,$0.02Eu^{3+}$ nanophosphors and (d–f) $Ca_{0.94}MoO_4$:$0.03Na^+$,$0.03Tb^{3+}$ under excitation of DUV light, respectively.

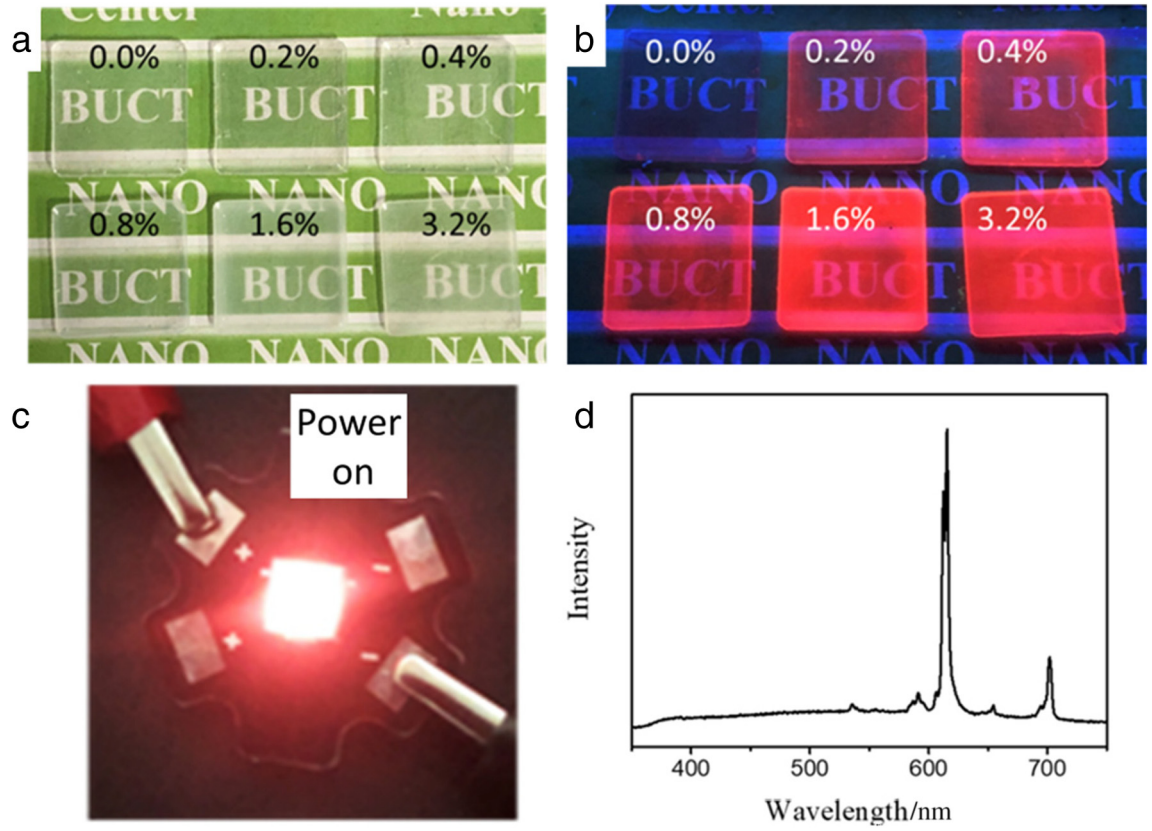

Fig.7. Photographs of silicone/$CaMoO_4$:Na^+,Eu^{3+} hybrid films with concentrations of $CaMoO_4$:Na^+,Eu^{3+} (0.0, 0.1wt%, 0.4wt%, 0.8wt%, 1.6wt%, 3.2 wt%) under (a)daylight and (b)DUV light excitation. (c)Photograph of a lighted LED lamp consisting of a DUV LED chip and silicone/$CaMoO_4$:Na^+,Eu^{3+} encapsulation layer. (d)Luminescence spectrum of the lighted LED lamp.

Acknowledgments

We are grateful for financial support from the National Key Research and Development Program of China(2017YFB0404302/2017YFB0404300), National Natural Science Foundation of China(21808009, 91934303), the Beijing Natural Science Foundation(2182051).

References

[1] S. van Loy, K. Binnemans, T. van Gerven, Mechanochemical-assisted leaching of lamp phosphors: A green engineering approach for rare-earth recovery, *Engineering* 4 (2018) 398–405.
[2] L. Zhang, J. Li, K. Liu, Recent advances in gadolinium-based MRI metal responsive agent, *Sci China Tech Sci* 61 (2018) 1329–1333.
[3] J. Lei, X. Guo, Q. Min, *et al.*, Brightening upconverting nanocrystals using laser-induced surface reconstruction, *Mater Today Nano* 8 (2019) 100055.
[4] L. Lin, X. Ma, S. Li, M. Wouters, V. Hessel, Plasma-electrochemical synthesis of europium doped cerium oxide nanoparticles, *Front. Chem. Sci. Eng.* 13 (2019) 501–510.
[5] Q. Zhan, H. Liu, B. Wang, *et al.*, Achieving high-efficiency emission depletion nanoscopy by employing cross relaxation in upconversion nanoparticles, *Nat. Commun.* 8 (2017) 1058.
[6] W. Shi, W. Lv, T. Sun, B. Zhang, Optoelectronic platform and technology, *Frontiers Inf Technol Electronic Eng* 20 (2019) 439–457.
[7] X. He, R. Tang, F. Yang, *et al.*, Zirconia quantum dots for a nonvolatile resistive random access memory device, *Front Inform Technol Electron Eng* 20 (2019) 1698–1705.
[8] T. Manohar, S.C. Prashantha, H.P. Nagaswarupa, *et al.*, White light emitting lanthanum aluminate nanophosphor: near ultra violet excited photoluminescence and photometric characteristics, *J. Lumin.* 190 (2017) 279–288.
[9] N. Susilo, S. Hagedorn, D. Jaeger, *et al.*, AlGaN-based deep UV LEDs grown on sputtered and high temperature annealed AlN/sapphire, *Appl. Phys. Lett.* 112 (2018), 041110.
[10] A.C. Duke, S. Hariyani, J. Brgoch, $Ba_3Y_2B_6O_{15}$:Ce^{3+}—A high symmetry, narrow-emitting blue phosphor for wide-gamut white lighting, *Chem. Mater.* 30 (2018) 2668–2675.
[11] S. Mitra, Y. Pak, N. Alaal, *et al.*, Novel P-type wide bandgap manganese oxide quantum dots operating at deep UV range for optoelectronic devices, *Adv Opt Mater* 7 (2019) 1900801.
[12] B.P. Singh, P.V. Ramakrishna, S. Singh, *et al.*, Improved photo-luminescence behaviour of Eu^{3+} activated $CaMoO_4$ nanoparticles via Zn^{2+} incorporation, *RSC Adv.* 5 (2015) 55977–55985.
[13] J. Shu, Z. Jia, E. Damiano, *et al.*, Charge compensations of $Eu^{2+}$and O_i^{2-}co-exist in Eu^{3+}:$CaMoO_4$single-crystal fibers grown by the micro-pulling-down method, *Cryst Eng Comm* 20 (2018) 6741–6751.
[14] Y. Xie, S. Ma, Y. Wang, *et al.*, Controlled synthesis and luminescence properties of $CaMoO_4$:Eu^{3+} microcrystals, *Opt. Mater.* 77 (2018) 13–18.
[15] D. Spassky, A. Vasil'Ev, A. Belsky, *et al.*, Excitation density effects in luminescence properties of $CaMoO_4$ and $ZnMoO_4$, *Opt. Mater.* 90 (2019) 7–13.
[16] R.L. Tranquilin, L.X. Lovisa, C.R.R. Almeida, *et al.*, Understanding the white-emitting $CaMoO_4$ Co-doped Eu^{3+}, Tb^{3+}, and Tm^{3+} phosphor through experiment and computation, *J. Phys. Chem. C* 123 (2019) 18536–18550.
[17] B.P. Singh, A.K. Parchur, R.S. Ningthoujam, *et al.*, Enhanced photoluminescence in $CaMoO_4$:Eu^{3+} by Gd^{3+} co-doping, *Dalton Trans.* 43 (2014) 4779–4789.
[18] Y. Zhai, X. Zhao, C. Liu, *et al.*, $CaMoO_4$:Dy^{3+},Eu^{3+} phosphors: microwave synthesis, characterization, tunable luminescence properties and energy transfer mechanism, *Optik* 164 (2018) 433–442.
[19] S. Dutta, S. Som, S.K. Sharma, Luminescence and photometric characterization of K^+ compensated $CaMoO_4$:Dy^{3+} nanophosphors, *Dalton Trans.* 42 (2013) 9654–9661.
[20] H.N. Luitel, R. Chand, T. Watari, $CaMoO_4$:RE^{3+},Yb^{3+},M^+ phosphor with controlled morphology and color tunable upconversion, *Displays* 42 (2016) 1–8.
[21] R. Wangkhem, T. Yaba, N. Shanta Singh, R.S. Ningthoujam, Red emission enhancement from $CaMoO_4$: Eu^{3+} by co-doping of Bi^{3+} for near UV/blue LED pumped white pcLEDs: Energy transfer studies, *J. Appl. Phys.* 123 (2018) 124303.
[22] Y. Ding, J. Liu, Y. Zhu, *et al.*, Brightly luminescent and color-tunable $CaMoO_4$:RE^{3+} (RE = Eu, Sm, Dy, Tb) nanofibers synthesized through a facile route for efficient light-emitting diodes, *J. Mater. Sci.* 53 (2018) 4861–4873.
[23] Y. Pu, J. Leng, D. Wang, J. Wang, N.R. Foster, J. Chen, Recent progress in the green synthesis of rare-earth doped upconversion nanophosphors for optical bioimaging from cells to animals, *Chin J Chem Eng* 26 (2018) 2206–2218.
[24] C. Ma, J. Su, B. Li, A. Herrmann, H. Zhang, K. Liu, Solvent-free plasticity and programmable mechanical behaviors of engineered proteins, *Adv. Mater.* (2020) https://doi.org/10.1002/adma.201907697.
[25] Z. Deng, L. Cao, F. Tang, B. Zou, A new route to zinc-blende CdSe nanocrystals: mechanism and synthesis, *J. Phys. Chem. B* 109 (2005) 16671–16675.
[26] D. Wang, J. Qian, F. Cai, *et al.*, 'Green'-synthesized near-infrared PbS quantum dots with silica-PEG dual-layer coating: Ultrastable and biocompatible optical probes for in vivo animal imaging, *Nanotechnology* 23 (2012) 245701.
[27] Y. Pu, L. Lin, D. Wang, J. Wang, J. Qian, J. Chen, Green synthesis of highly dispersed ytterbium and thulium co-doped sodium yttrium fluoride microphosphors for in situ light upconversion from near-infrared to blue in animals, *J Colloid Interf Sci* 511 (2018) 243–250.

[28] Y. Pu, J. Leng, D. Wang, J. Wang, N.R. Foster, J. Chen, Process intensification for scalable synthesis of ytterbium and erbium co-doped sodium yttrium fluoride upconversion nanodispersions, *Powder Technol.* 340 (2018) 208–216.
[29] Y. Jiao, Y. Pu, J. Wang, D. Wang, J. Chen, Process intensified synthesis of rare-earth doped β-$NaYF_4$ nanorods toward gram-scale production, *Ind. Eng. Chem. Res.* 58 (2019) 22306–22314.
[30] X. He, Z. Wang, Y. Pu, *et al.*, High-gravity-assisted scalable synthesis of zirconia nanodispersion for light emitting diodes encapsulation with enhanced light extraction efficiency, *Chem. Eng. Sci.* 195 (2019) 1–10.
[31] Z. Wang, J. Shi, D. Wang, *et al.*, Metal-free catalytic oxidation of benzylic alcohols for benzaldehyde, *React Chem Eng* 4 (2019) 507–515.
[32] H.G. Liao, L. Cui, S. Whitelam, *et al.*, Real-time imaging of Pt_3Fe nanorod growth in solution, *Science* 336 (2012) 1011–1014.
[33] L. Guo, J. Wu, J. Li, Complexity at mesoscales: A common challenge in developing artificial intelligence, *Engineering* 5 (2019) 924–929.
[34] J. Li, Exploring the logic and landscape of the knowledge system: multilevel structures, each multiscaled with complexity at the mesoscale, *Engineering* 2 (2016) 276–285.
[35] W.L. Huang, J. Li, X. Chen, 110th anniversary: mesoscale complexity—To dodge or to confront? *Ind. Eng. Chem. Res.* 58 (2019) 12478–12484.
[36] W. Bu, Z. Chen, F. Chen, J. Shi, Oleic acid/oleylamine cooperative-controlled crystallization mechanism for monodisperse tetragonal bipyramid $NaLa(MoO_4)_2$ nanocrystals, *J. Phys. Chem. C* 113 (2019) 12176–12185.
[37] S. Cui, X. He, D. Wang, *et al.*, Tuning the doping of europium in gadolinium borate microparticles at mesoscale toward efficient production of red phosphors, *ACS Omega* 4 (2019) 14497–14502.